The Journal of Physical Chemistry A

 VOLUME 103, NUMBER 8, FEBRUARY 25, 1999

ARTICLES

Vibrational Energy Redistribution in Polyatomic Liquids: Ultrafast IR−Raman Spectroscopy of Nitromethane

John C. Deàk, Lawrence K. Iwaki, and Dana D. Dlott*

Department of Chemistry, University of Illinois at Urbana-Champaign, Box 01-6 CLSL, 600 S. Mathews Avenue, Urbana, Illinois 61801

Received: October 6, 1998

Ultrafast anti-Stokes Raman spectroscopy of liquid nitromethane (NM) after mid-IR excitation in the C−H stretching region (∼3000 cm^{-1}) is used to study vibrational energy redistribution with ∼1 ps time resolution. Both vibrational energy relaxation (VER) and vibrational cooling (VC) are discussed. Raman probing of CCl_4 mixed with the NM is used to monitor the buildup of excitation in the bath of collective lower frequency excitations (phonons). Combining the intramolecular and bath data, a new and intuitive way of visualizing VC in a polyatomic liquid is presented. In NM, VC occurs in three stages. First, energy deposited in the C−H stretch (and a small amount in first overtones of NO_2 stretching and CH bending vibrations) is redistributed to every other vibration in a few picoseconds. Second, the higher energy daughter vibrations of the C−H stretch decay (∼1600−1400 cm^{-1}) relax by populating the lower energy vibrations (∼1100−480 cm^{-1}) in ∼15 ps. Third, the lower energy vibrations excited in the first two stages relax by exciting the bath in 50−100 ps. Although the average vibrational energy decreases with time, this process differs from the usual vibrational cascade description of VC.

1. Introduction

With recent improvements in ultrashort infrared pulse generation, vibrational energy relaxation (VER) of polyatomic liquids has again become a timely topic. In this paper, we discuss VER and vibrational cooling (VC) of liquid nitromethane (NM) at ambient temperature. VER refers to a single energy relaxation step, where a parent intramolecular vibration creates some combination of intramolecular daughter vibrations and collective excitations of the bath (phonons). VC is a multistep process usually involving several VER steps, in which a molecule loses all its excess vibrational energy. VER of NM has been studied previously,[1−3] but not with the time resolution and sensitivity of the present work.

The multiple roles of VER in liquid state dynamics have been discussed recently.[4,5] Experimental and theoretical studies of VER in liquids have been reviewed extensively.[6−10] VER plays several well-known roles in liquid-state chemical reaction dynamics. For example, in activated barrier crossing, a solute is first activated by taking up vibrational energy from the solvent (multiphonon up-pumping). Then the barrier crossing is modulated by VER.[5,11,12] Finally, the appearance of products coincides with the loss of the vibrational energy via VER.[5] A lesser known, but immensely practical, application of VER studies relates to the shock initiation and detonation of high explosives.[13−15] Initiation involves energy transfer from a shock to a molecule's vibrations.[13,14,16−19] Detonation involves chemistry in an environment where practically every molecule is vibrationally excited.[15,20]

Recently, there has been a revival of the IR−Raman method, where an intense mid-IR pulse excites a higher frequency vibrational fundamental (usually a C−H stretch) and a visible

* To whom correspondence should be addressed. E-mail: d-dlott@uiuc.edu.

10.1021/jp9839899 CCC: $18.00
Published on Web 02/05/1999

TABLE 1: Nitromethane Vibrations (C_{2v})

mode	frequency (cm^{-1})	symmetry	assignment	observation frequency (cm^{-1})	$\eta'^{-1\,a}$	lifetime (ps) of $v = 1$
ν_1	3050	B_2	$\nu_a(CH_3)$	2968	0.17	
ν_2	3050	B_1	$\nu_a(CH_3)$	2968	0.17	
ν_3	2968	A_1	$\nu_s(CH_3)$	2968	1.00	2.6 ± 0.1
ν_4	1560	B_1	$\nu_a(NO_2)$	1560	0.10	15 ± 3
ν_5	1426	B_2	$\delta_a(CH_3)$	1560/1400	0.03/0.10	
ν_6	1426	B_1	$\delta_a(CH_3)$	1560/1400	0.03/0.10	
ν_7	1402	A_1	$\delta_s(CH_3)$	1400	0.19	18 ± 2
ν_8	1379	A_1	$\nu_s(NO_2)$	1400	0.15	18 ± 2
ν_9	1125	B_2	$\rho(CH_3)$			
ν_{10}	1104	B_1	$\rho(CH_3)$	1100	0.03	30 ± 5
ν_{11}	918	A_1	$\nu_s(CN)$	918	0.20	32 ± 3
ν_{12}	657	A_1	$\delta_s(NO_2)$	657	0.08	~ 50
ν_{13}	607	B_2	$\rho(NO_2)$	657	0.01	
ν_{14}	480	B_1	$\rho(NO_2)$	480	0.02	~ 50
ν_{15}	~ 60	A_2	$\tau(CH_3)$			

[a] η and η' convert anti-Stokes intensities to relative changes in vibrational populations (see eqs 5 and 7). The values are given relative to the ν_3(C−H) stretch pumped by the laser.

probe pulse generates anti-Stokes transients whose amplitudes are proportional to instantaneous vibrational populations. The revival is due to improvements in higher repetition rate solid-state lasers. In 1995 our group studied NM[2] with an IR−Raman system with an ∼80 ps time response full width at half-maximum (fwhm). In 1995 and 1997, Graener et al. studied CH_2Cl_2[21] and $CHCl_3$[22] using a laser with ∼1 ps time resolution. About that time, our group began development of an improved spectrometer that provides ∼1 ps resolution, based on Ti: sapphire technology,[23] which was used for preliminary studies[23] of NM and more extensive studies[24,25] of CH_3CN.

In the present work, we have reexamined NM. NM is an interesting system from the theoretical point of view. So far, most theoretical treatments deal with either diatomic molecules[9,26,27] or larger polyatomic molecules.[28,29] To treat polyatomics, a perturbative approach is ordinarily used. The anharmonic interaction potential is expanded in powers of the coordinates. The lowest order processes, usually involving cubic or quartic anharmonic coupling are then considered[29] to dominate. These lower-order processes lead to "ladder" VER processes, where VER occurs by exciting a lower energy vibration and a small number of phonons.[28,29] When ladder processes dominate, VC occurs by a vibrational cascade.[30,31] To treat diatomics, perturbative approaches are usually not accurate. Instead, the frequency-dependent friction is computed at the oscillator frequency, from the Fourier transform of the force−force correlation function.[27,32] VER in NM is therefore particularly interesting because it obviously cannot be treated by the diatomic approach, and yet it is a small enough molecule that, as shown here, rather high-order anharmonic coupling terms (fourth to sixth order and possibly higher) from the perturbative approach are necessary. In our previous work,[2,23] VER in NM was described as occurring via vibrational cascade. Now that we can observe all relevant time scales with greater sensitivity, we will show that vibrational cascade is a too simplistic description of the actual VC process.

NM is also interesting in light of its role as a high explosive and the importance of VER in high explosive processes.[13−15,17,19,33,34] VER plays several important roles in the initiation[13,14] and detonation[15] of high explosives. We will discuss to what extent the VER properties of NM differ from nonexplosives with similar structure (e.g., CH_3CN), and speculate about the relationships between VER and explosive properties of NM.

In the rest of this paper, we first review the vibrational spectroscopy of NM. In contrast to CH_2Cl_2 and $CHCl_3$ studied previously, NM introduces a new level of complexity because it is not possible to individually resolve every vibrational transition (spectral congestion). Methods for interpreting IR−Raman data of congested systems are discussed. A method described earlier[22] for converting IR−Raman transients into populations will be extended to deal with spectral congestion. In addition, a new technique is introduced to monitor the buildup of excitation in the bath, by adding a molecular thermometer, CCl_4, to the NM. Combining occupation number data with bath buildup data, a new and intuitive way of visualizing VER can be realized.

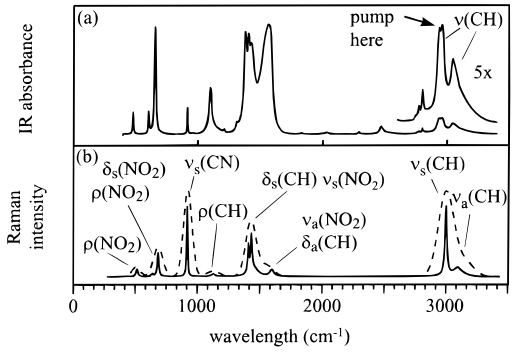

Figure 1. IR absorption (top) and Stokes Raman spectra (bottom, corrected for spectral responsivity) of nitromethane (NM). The solid Raman spectrum with ∼5 cm^{-1} resolution was obtained with a narrow band laser, and the dashed Raman spectrum was obtained using the picosecond probe pulse.

2. Vibrational Spectroscopy of Nitromethane (NM)

The vibrational spectroscopy of NM has been discussed previously.[35−37] The discussion here reviews essential elements needed to understand the VER measurements. Nitromethane belongs to point group[38] C_{2v}. The fifteen NM vibrations, their numbering scheme, their symmetries, and assignments are given in Table 1. Figure 1 shows IR and Stokes Raman spectra of NM, where the instrument resolution is better than the natural line widths of NM (experimental details in the next section). When the ultrafast laser is used for Raman scattering, the resolution is lowered due to the ∼50 cm^{-1} bandwidth of the probe pulses.[23] The lower resolution Raman spectrum in Figure 1b uses the ultrashort probe pulses. In three regions of the Raman spectrum, ∼1560, ∼1400, and ∼657 cm^{-1}, multiple vibrational transitions are observed, most of which cannot be resolved even in the higher resolution spectrum.

In VER experiments, the mid-IR pulses were tuned to the maximum absorption in the C−H stretching region, near 2970 cm^{-1}, as indicated in Figure 1. At this wavelength, the pump pulse is predominantly absorbed by the symmetric C−H stretching mode, ν_3, at 2970 cm^{-1}, but also somewhat by the antisymmetric C−H stretching transitions, ν_1 and ν_2. Overtones of lower frequency transitions buried in the C−H stretch absorptions may also be excited, especially the first overtones of the antisymmetric CH_3 bending and NO_2 stretching vibrations.

3. Experimental Section

The experimental setup for IR−Raman measurements was discussed previously.[23] The IR pump pulses ($\lambda = 3.37$ μm or 2970 cm^{-1}, 35 cm^{-1} bandwidth, ~1 ps, 40 μJ, Gaussian beam radius = 100 μm) and visible Raman probe pulses ($\lambda = 532$ nm or 18 800 cm^{-1}, 50 cm^{-1} bandwidth, 0.8 ps, 20 μJ, Gaussian beam radius = 80 μm) are generated at a repetition rate of 1 kHz by a two-color optical parametric amplifier (OPA) pumped by a picosecond Ti:sapphire laser. The sample is an ~150 μm thick jet of NM (Aldrich, reagent grade) or NM diluted with CCl_4 (Aldrich), 1:3 by volume. In neat NM, the pump pulses produce a temperature jump[24] on the order of $\Delta T = 10$ K, which represents a spatial average over the probed volume.[39] In the solution, the temperature jump is about one-fourth this value.

Infrared absorption spectra with 2 cm^{-1} resolution (Figure 1a) were obtained in a thin cell with CaF_2 windows using a Fourier transform IR spectrometer. The higher resolution (~5 cm^{-1}) Raman spectrum in Figure 1b was obtained using an optical array detector, a continuous wave frequency-doubled Nd:YVO_4 laser, which produces a narrow spectral output, and a narrower entrance slit on the spectrograph. The lower resolution (~50 cm^{-1}) Raman spectrum in Figure 1b is obtained under the conditions used for time-resolved measurements. The broader band picosecond probe pulses are used, and to transmit this larger bandwidth to the photomultiplier, the spectrometer slits are opened to ~600 μm. A frequency-dependent factor needed to correct for the spectral sensitivity of the spectrometer plus detector (optical array detector or photomultiplier) was determined using a calibrated 3145K blackbody source. The spectral band-pass of the spectrometer was determined using narrow-line atomic emission from a spectral calibration lamp.

4. Anti-Stokes Signals and Populations

In this section, we discuss how to convert anti-Stokes transients into populations. Anti-Stokes transients are measured by setting the monochromator to a particular observation frequency ν_{obs} with a detection bandwidth $\Delta\nu_s$ set by the slit width. The detection bandwidth function $S(\nu_{obs},\Delta\nu_s)$ was roughly a Gaussian with a 3.8 nm fwhm. In some cases the monochromator with this spectral bandwidth sees only a single transition. In two cases, there are congested spectral regions where multiple transitions with roughly equal amplitudes are observed. These are near 1400 cm^{-1}, where there are four intrinsically unresolved transitions $\nu_5-\nu_8$, which are C−H bending and symmetric NO_2 stretching transitions, and near 1560 cm^{-1}. At 1560 cm^{-1}, the antisymmetric NO_2 stretching vibration ν_4 is observed together with a contribution from the more intense ~1426 cm^{-1} antisymmetric C−H bending transitions $\nu_5-\nu_6$. There are two regions where multiple transitions are observed, but only one dominates. These are near 2970 cm^{-1}, where all three C−H stretching transitions $\nu_1-\nu_3$ are seen, but ν_3 dominates, and near 657 cm^{-1}, where NO_2 rocking and symmetric bending transitions ν_{12} and ν_{13} are seen, but ν_{12} dominates.

As previously described by[22] Graener et al., a population change can be found by combining anti-Stokes transient data with Raman cross-section data from a Stokes spectrum. The Stokes intensity of the *i*th transition, corrected for the spectral response of the instrument, at frequency ν_i is[22]

$$I_i^{St} = \text{const}\, N_0[1 - \exp(-h\nu_i/kT)]^{-1}\, g_i\sigma_{Ri}(\nu_L - \nu_i)^4 \quad (1)$$

where N_0 is the molecular number density, g_i is the degeneracy, σ_{Ri} is the Raman cross-section, and ν_L is the laser frequency. The constant in eq 1 depends on details of the Raman apparatus.

The anti-Stokes transient from the *i*th transition, multiplied by a factor that corrected for the relative spectral sensitivity of the ultrafast spectrometer, is denoted $\Delta I_i^{AS}(t)$. The delta indicates that the ambient background anti-Stokes signal (if any) is subtracted off. $\Delta I_i^{AS}(t)$ is related to the time-dependent population change $\Delta n_i(t)$ by[22]

$$\Delta I_i^{AS}(t) = \text{const}'\, \Delta n_i(t) g_i\sigma_{Ri}(\nu_L + \nu_i)^4 \quad (2)$$

where the constant depends on details of the IR−Raman setup.

Population changes are computed relative to the population of a reference transition at a particular time t_0, $\Delta n_0(t_0)$. Usually, the reference transition will be the transition pumped by the laser (here a C−H stretch), t_0 is the time the population is maximum, and the corresponding reference anti-Stokes intensity (not a function of time) is $\Delta I_0^{AS}(t_0)$. Introducing the reference transition lets the constants in eqs 1 and 2 cancel so

$$\frac{\Delta n_i(t)}{\Delta n_0(t_0)} = \eta_i \frac{\Delta I_i^{AS}(t)}{\Delta I_0^{AS}(t_0)} \quad (3)$$

where η_i is the factor that converts the anti-Stokes transient to an occupation number, taken relative to the occupation numberof the level pumped by the laser,

$$\eta_i = \frac{I_0^{St}(\nu_L - \nu_i)^4(\nu_L + \nu_0)^4(1 - e^{-h\nu_0/kT})}{I_i^{St}(\nu_L + \nu_i)^4(\nu_L - \nu_0)^4(1 - e^{-h\nu_i/kT})} \quad (4)$$

and I_0^{St} and I_i^{St} are intensities (integrated across the Raman line) obtained from a Raman spectrum that can resolve the natural Raman line shapes.

Sometimes anti-Stokes transients are observed from several vibrations simultaneously, due to spectral congestion. How much of each transition is seen may depend on the probe pulse bandwidth ($\Delta\nu_{pr}$), the Raman cross-sections σ_{Ri}, the observation frequency ν_{obs}, and the spectral band-pass function $S(\nu_{obs},\Delta\nu_S)$, which depends on the spectrometer band-pass $\Delta\nu_s$ and the observation frequency. To deal with this situation, we use a time dependent change in *average occupation number* $\Delta\bar{n}(t)$,

$$\Delta\bar{n}(t) = \frac{\sum_i \Delta n(t)\eta_i'^{-1}}{\sum_i \eta_i'^{-1}} \quad (5)$$

$$\frac{\Delta\bar{n}(t)}{\Delta n_0(t_0)} = \frac{\Delta I^{AS}(t,\nu_{obs})}{\Delta I_0(t_0)} \frac{1}{\sum_i \eta_i'^{-1}} \quad (6)$$

where the conversion factor (η_i') now depends on the experimental parameters $\Delta\nu_{pr}$, $\Delta\nu_S$, and ν_{obs}. This factor is obtained

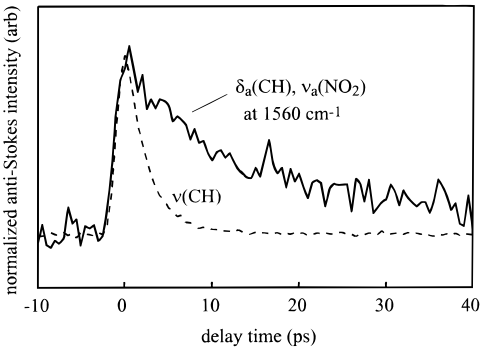

Figure 2. Anti-Stokes transients for ν_3(C−H) stretch (dashed line) and for a mixture of antisymmetric NO_2 stretch and C−H bends monitored at 1560 cm^{-1} (solid line). The transients are normalized to the same height. The ∼1 ps rise of both transients is determined by the pump pulse duration. Both C−H stretch fundamentals and NO_2 stretch and C−H bend first overtones are pumped by the mid-IR laser.

as follows. First the higher resolution Raman spectrum is convolved with the probe pulse spectrum. Then the result is filtered by the band-pass function. In this case, η'_i is given by

$$\eta'_i = \eta_i \frac{\int g'_L(\nu_L + \nu_i,\Delta\nu_i)\, S(\nu_L + \nu_i,\Delta\nu_S)\, d\nu}{\int g'_L(\nu_L + \nu_0,\Delta\nu_0)\, S(\nu_L + \nu_0,\Delta\nu_S)\, d\nu} \qquad (7)$$

where the function $g'_L(\nu_L + \nu_i,\Delta\nu_i)$ is the convolution of the probe pulse spectrum with a line shape function $g_L(\nu,\Delta\nu)$ used to represent the Raman spectrum. The relative sensitivity of the IR−Raman instrument to the populations of the individual nitromethane vibrations is thus given by $(\eta'_i)^{-1}$.

Using the experimentally measured spectral band-pass function, probe pulse spectrum, and Stokes Raman spectrum, we computed η' (eq 8) relative to the ν_3(C−H) stretch for NM at various observation wavelengths. The results are given in Table 1. When ν_{obs} is set to 1560 cm^{-1}, the anti-Stokes transient is ∼40% NO_2 antisymmetric stretch ν_4, and ∼60% antisymmetric C−H bending transitions ν_5 and ν_6. When ν_{obs} is set to 1400 cm^{-1}, the anti-Stokes transient is ∼30% antisymmetric C−H bending transitions ν_5 and ν_6, ∼40% symmetric C−H bending transition ν_7, and ∼30% symmetric NO_2 stretching transition ν_8.

Since $\Delta\bar{n}(t)$ is an average property, readers are cautioned that it could be a bit misleading. For example, if a weaker and a more intense transition are monitored simultaneously, one may not be able to distinguish between a large population change in the weaker transition or a small population change in the more intense transition. Vibrational transitions whose spectra overlap significantly are probably anharmonically coupled to each other, in which case energy would be redistributed among them on the time scale[10,40] of vibrational dephasing, T_2. In polyatomic liquids at ambient temperature, $T_2 \ll T_1$, where T_1 is the energy relaxation time constant, so in most cases we expect energy to be redistributed among overlapping transitions faster than it can decay away. When that occurs, the average population is certainly a meaningful and useful quantity.

5. Results

A. VER of Neat Nitromethane. Anti-Stokes transients from NM after C−H stretch pumping are shown in Figures 2−4. Prior to the arrival of the mid-IR pump pulse at $t = 0$, the anti-Stokes intensity is proportional to the ambient (294 K) vibrational population. The ambient background is subtracted from the data in Figures 2−4. All the anti-Stokes transients in Figures 2−4

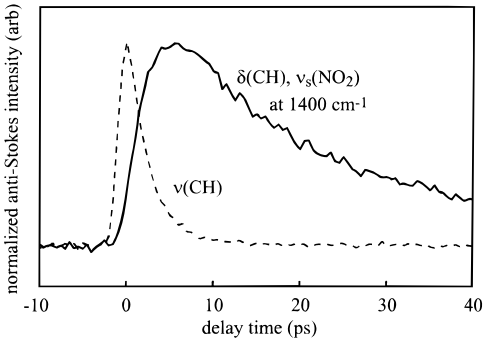

Figure 3. Normalized anti-Stokes transients for C−H stretch (dashed line) and for a mixture of symmetric NO_2 stretch and C−H bends monitored at 1400 cm^{-1} (solid line). The rise of the 1400 cm^{-1} signal occurs on the 2.6 ps time scale of C−H stretch decay.

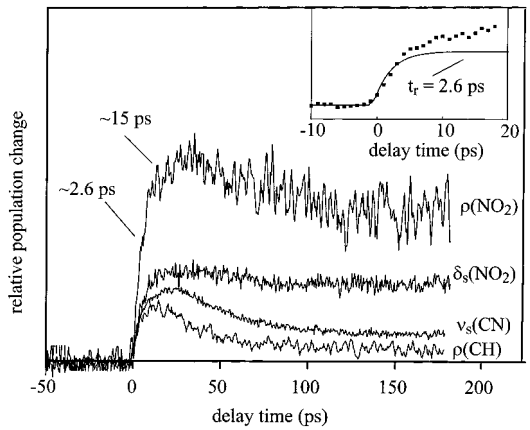

Figure 4. Relative population changes of four lower energy vibrations $\nu_{10}-\nu_{12}$ and ν_{14}, obtained by normalizing the anti-Stokes transients using eqs 3, 4, and 7. The vibrations are ν_{10} ρ(CH), ν_{11} ν_s(CN), ν_{12} $\delta_s(NO_2)$, and ν_{14} $\rho(NO_2)$. The $\delta_s(NO_2)$ transient has an ∼10% contribution from ν_{13} $\rho(NO_2)$. All transients show a two-part rise, with the faster part occurring on the 2.6 ps time scale and the slower part on the ∼15 ps time scale, and decays on the 30−50 ps time scale. The inset shows the fast part of the ν_{11} rise fit with a 2.6 ps exponential.

decay back to the baseline (C−H stretch) or to a plateau representing a new equilibrium at a temperature ∼10 K greater than the ambient. All of the anti-Stokes transients appear to attain the new equilibrium by ∼150 ps, since the signals were observed to remain constant from 150 ps out to the maximum delay available with our apparatus, ∼1 ns. The time constant for the VC process will be taken to be the earliest time this new equilibrium is observed, i.e., ∼150 ps.

The anti-Stokes transients at 2970 and 1560 cm^{-1} are compared in Figure 2. The transients are normalized to be the same height. The 2970 cm^{-1} transient reflects mainly ν_3 population. The 1560 cm^{-1} transient is a mixture of antisymmetric C−H bend and NO_2 stretch. Both signals rise with the instrument response time (∼1 ps). The C−H stretch decay is a single exponential, within experimental error. The VER lifetime is 2.6 ps. The 1560 cm^{-1} decay becomes a single exponential after the first few picoseconds, and the decay constant is 15 ± 3 ps. The VER lifetimes measured here are summarized in Table 1. We note these results indicate the Raman line width due to lifetime broadening is only a small fraction of the total line width,[41−44] which is dominated by pure dephasing (the cited authors use the term "vibrational relaxation" to refer to pure dephasing).

The 1400 cm^{-1} transient, a mixture of C−H bending and NO_2 stretching transitions, is compared to the ν_3(C−H) stretch signal in Figure 3. In contrast to the 1560 cm^{-1} transient in

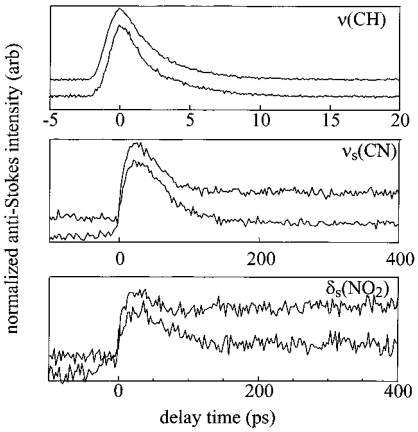

Figure 5. Anti-Stokes transients for three NM vibrations in neat NM and in NM:CCl_4 solution (1:3). The neat NM transients are offset above the CCl_4 solution transients. Adding CCl_4 lowers the plateau at longer time by reducing the temperature jump. The shorter time vibrational relaxation is unaffected by adding CCl_4.

Figure 2, which rises with the ∼1 ps instrument response, the rise of the 1400 cm^{-1} transient is clearly slower. The rise mirrors the 2.6 ps decay of the ν_3(C−H) stretch. The decay of the 1400 cm^{-1} transient is a single exponential. The VER lifetimes for transitions at 1400 cm^{-1} are 18 ± 2 ps.

Figure 4 shows anti-Stokes transients from four lower energy vibrations, ν_{10}, ν_{11}, ν_{12}, and ν_{14}. These transients have been scaled using eq 3 and the factors listed in Table 1. The rising edge of all four transients in Figure 4 has a faster and a slower part. The faster part occurs on the 2.6 ps time scale of the C−H stretch decay and the slower part on the ∼15−18 ps time scale of the decay of the C−H bends and NO_2 stretches. To better show the two-part rise, the inset shows an expanded view of the first 20 ps of the ν_{11} transient. The solid curve in the inset is a computed rise with a 2.6 ps time constant. The ν_{11} transient follows this computed rise for the first few picoseconds, but then it breaks away due to the slower part of the rise. The amplitudes of the fast part of the rise are identical for ν_{10}−ν_{12}, but the amplitude of the fast rise for ν_{14} is twice as large as the others. The VER lifetimes of ν_{10} and ν_{11} are ∼30 ps. The VER lifetimes of ν_{12} and ν_{14} are hard to determine accurately, but they seem a bit slower, ∼50 ps. The ∼50 ps decay lifetime of ν_{12} in CCl_4 solution (Figure 5 discussed below) is much more clearly evident.

B. VER of Nitromethane in CCl_4. In the NM−CCl_4 solutions, only NM is pumped because CCl_4 is transparent at 2970 cm^{-1}. The same amount of heat is dissipated in a larger volume, the bulk temperature jump is smaller, and the long-time plateau is lower. Figure 5 compares data for three NM vibrations in neat NM and in CCl_4 solution. In solution, the signal-to-noise ratio is a bit worse. The C−H stretching signals are essentially identical. The ν_{11}(C−N) stretch and the ν_{12}(NO_2) bend signals rise and fall with the same time constants observed in neat NM until the anti-Stokes transients begin to plateau. In solution, the transients fall a bit farther and level out at a lower value, due to the smaller temperature jump.

The 315 cm^{-1} transition of CCl_4 in the NM:CCl_4 solution, corresponding to a Cl−C−Cl bending vibration, was monitored following excitation of the NM C−H stretching vibration. The CCl_4 signal is plotted in Figure 6. There is essentially no excitation of the CCl_4 vibration during the first 20 ps. The CCl_4 anti-Stokes transient rises on the 20−150 ps time scale, and it levels out by 150 ps.

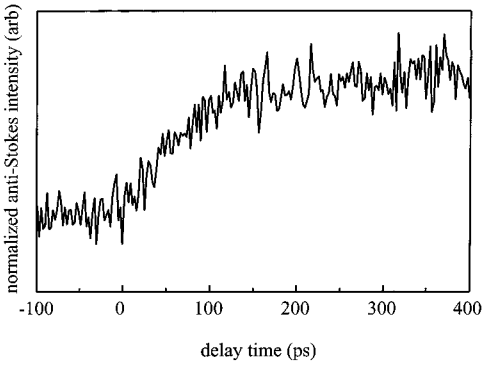

Figure 6. Anti-Stokes transient of the 315 cm^{-1} mode of CCl_4 after C−H stretch pumping of NM in the NM:CCl_4 solution, which tracks the buildup of bath excitation.

6. Discussion

A. Brief Summary of Experimental Results. All of the VER processes seen in nitromethane can be roughly described by four time constants: 1, 2.6, ∼15, and 30−50 ps. The rise of the pumped C−H stretch and the 1560 cm^{-1} transients occurs on the 1 ps time scale of the mid-IR pump pulse. These vibrations must be directly excited by the laser. C−H stretch population decays with a 2.6 ps time constant. The 1400 cm^{-1} transient rises with this same 2.6 ps time constant. The 1560 and 1400 cm^{-1} transients (ν_4−ν_8) decay with an ∼15 ps time constant. A two-part rise with the 2.6 and 15 ps time constants is seen in every transition below 1400 cm^{-1}. The ν_{10}, ν_{11}, ν_{12}, and ν_{14} signals all have relatively long lifetimes in the 30−50 ps range (∼30 ps for ν_{10} and ν_{11} and ∼50 ps for ν_{12}, and ν_{14}). The VC process is complete by ∼150 ps (Figures 4−6). The earlier study[2] of NM with 80 ps time resolution is seen to be generally consistent with the present work. Earlier, the VC process was said to last ∼200 ps. The existence of an ∼15 ps time constant was inferred from the time shift of the peaks of some of the other anti-Stokes transients. The rather long lifetimes (∼50 ps) of the lowest frequency NM vibrations are consistent with measurements of multiphonon up-pumping in NM.[1] Of course the earlier study saw few of the details and none of the fast processes seen here.

B. Interpretation of the CCl_4 Experiments. We wish to use the CCl_4 as a "molecular thermometer"[45] to monitor the rise of bath excitation as the NM undergoes vibrational cooling. Ideally, the molecular thermometer would have two properties: (1) the thermometer would not significantly perturb the VC process; (2) the thermometer's vibrations would come into equilibrium with the bath fast enough to monitor even the fastest VC processes.

First we consider the effects of CCl_4 on vibrational cooling of NM. CCl_4 vibrations could become excited by NM vibrational cooling in two ways[46,47] termed *direct* or *indirect*. Direct refers to transfer from an NM vibration directly to a vibration of a CCl_4 molecule, which is most likely in contact with NM. If direct transfer dominated, CCl_4 would significantly perturb the lifetimes of some NM vibrations. Indirect transfer is a two-step process. First, VC of NM excites phonons in the bath. Second, these phonons excite vibrations of CCl_4 molecules by multiphonon up-pumping. The CCl_4 in this case need not be in contact with the NM. We see from Figure 5 that CCl_4 reduces the temperature jump but otherwise has no effect on the rates and amplitudes of VER in NM. Keep in mind we could not monitor *every* NM transition (e.g., the ν_{14} vibration is obscured by an intense CCl_4 transition). Thus we believe indirect processes dominate. In indirect transfer, effects of CCl_4 on NM

could be mild, only to the extent that adding CCl_4 affects the phonon density of states and the coupling to the phonon bath.[29,48,49] Although the sample was diluted with CCl_4, the concentration of NM remained quite large (~5 M). In fact, the sample may well consist primarily of NM aggregates, in which case the lack of a big effect seen in Figure 5 is hardly surprising. If the level of dilution were increased enough that NM was present only as isolated molecules in a sea of CCl_4 (e.g., 10^{-3} M), it is possible that CCl_4 might have a more noticeable effect on the VER.

Second, we consider the response time of the CCl_4. Figure 6 shows the CCl_4 vibration comes to equilibrium at the same time as NM, ~150 ps, which shows the CCl_4 is tracking the slower parts of the VC process. Although we cannot say exactly how fast the CCl_4 can respond in NM, we have some relevant preliminary results on CCl_4 in other polyatomic liquids. The most interesting result comes from CCl_4 in methanol,[50] because methanol VC, occurring in 15−20 ps, is considerably faster than in NM. In addition, we can monitor three prominent CCl_4 Raman transitions, at 315, 459, and 790 cm^{-1} (NM transitions obscure all but the 315 cm^{-1} CCl_4 transition studied here). We find in methanol that CCl_4 vibrational excitation builds up *simultaneously in all three* CCl_4 transitions in about 20 ps. These results indicate that the response time of the CCl_4 molecular thermometer is at least ~20 ps, and in fact might be even faster. In addition, they indicate it does not matter which of the three prominent Raman transitions are monitored.

Assuming the up-pumping of CCl_4 is not radically different in NM, we interpret Figure 6 as follows. Figure 6 shows almost no CCl_4 excitation during the first 10 ps, and at ~30 ps, the level of CCl_4 excitation is less than one-third of the final level. We conclude that in NM, the first fast VER step of decay of the C−H stretch on the 2.6 ps time scale dissipates almost no energy to the bath (few phonons are generated). That contrasts with our work on acetonitrile,[24] where C−H stretch decay dissipates ~1500 cm^{-1} to the bath in a few picoseconds. We also conclude the ~15 ps time scale decay of transitions at 1560 and ~1400 cm^{-1} dissipates about one-third of the total energy to the bath, which is consistent with the idea that relaxation of the ~1500 cm^{-1} vibrations occurs by exciting ~1000 cm^{-1} vibrations. Figure 6 shows that most of the energy buildup in the bath occurs on the 50−100 ps time scale, which is associated with the relaxation of lower energy vibrations into the bath.

C. Pumping Fundamentals and Overtones Simultaneously. In several earlier works,[10,40,51] the claim was made that C−H stretch decay occurred mainly by coupling (via Fermi resonance) to first overtones of C−H bending transitions whose fundamentals are in the 1500 cm^{-1} range. That is clearly not the case.[24] The mid-IR pulse simultaneously pumps an admixture of C−H stretching transitions and those excitations that are observed at ~1560 cm^{-1}, as shown by the instantaneous rise (limited by the pump pulse) of both transients in Figure 2. At ~1560 cm^{-1}, our apparatus monitors antisymmetric C−H bends $\delta_a(CH_3)$ and the antisymmetric NO_2 stretch $\nu_a(NO_2)$. Energy conservation necessitates that we must pump the first overtones of these transitions. Because the anharmonicity is less than our spectroscopic resolution, first overtone excitation looks to our apparatus like excitation of the fundamental with twice the amplitude.[22]

An interesting feature of the data is although the C−H stretch and overtone excitation data in Figure 2 track each other for the first few picoseconds, the 1560 cm^{-1} transient decays much slower than the C−H stretch. That can be understood if the latter part of the 1560 cm^{-1} transient is associated with *fundamental* excitations of the asymmetric C−H bend and NO_2 stretch, which are produced when the coupled C−H stretch and overtone excitations undergo VER. We have confidence in this assignment, because Fayer and co-workers[52] have used infrared pump−probe techniques to measure the lifetime of the 1560 cm^{-1} NO_2 stretch fundamental. In those experiments, the intensity and bandwidth of the pump pulses was controlled to produce only fundamental excitations. The lifetime they found, 15 ps, is identical to that seen in Figure 2. The 15 ps decay cannot be due to overtone decay, since the decay rate of a first overtone excitation must *at minimum* be twice as large as the same fundamental. That is true regardless of the VER mechanism, because the amplitude for annihilating a first overtone is always larger than the amplitude for annihilating a fundamental.[28]

Consequently, the 1560 cm^{-1} anti-Stokes transient in Figure 2 is a bit complicated. During the first few picoseconds, the anti-Stokes signal at 1560 cm^{-1} arises from first overtones. Because these overtones are strongly coupled to the C−H stretch fundamental (i.e., the magnitude of the coupling is greater than the inverse lifetime), all these states decay with the same 2.6 ps time constant. A portion of the decay populates fundamentals of the C−H bend and NO_2 stretch, which are seen by our apparatus at the same 1560 cm^{-1} observation wavelength.

D. Decay of the C−H Stretch and Coupled Overtones: The Fastest VER Process. The excitations pumped by the laser decay with a 2.6 ps lifetime. An identical 2.6 ps rise is seen *in every transition probed*. (The 2.6 ps process is not directly observed in the 1560 cm^{-1} transient, but above we discussed how the 2.6 ps buildup of fundamental excitation was obscured by the decay of overtone excitations.) Clearly, the C−H stretch energy is redistributed *throughout virtually all NM vibrations* (we cannot be certain about ν_9 or ν_{13}). The CCl_4 results (Figure 6) show that the C−H stretch decay is *mainly intramolecular*, since it is associated with *little or no energy buildup in the bath*.

The C−H stretch decay is complicated because so many processes occur simultaneously. We wish to emphasize the term "mainly intramolecular" should not be taken to imply the bath plays no role, as would be the case for isolated molecule intramolecular vibrational relaxation.[53−55] The bath actually plays two roles. First, the bath modulates NM vibrational transition frequencies, which broadens the transitions. With the broadened transitions, it becomes easier to find energy-conserving VER pathways.[28,29] Second, VER might involve the bath accepting or donating a bit of energy,[29] e.g., ±100 cm^{-1}, which is not enough to be seen with our present sensitivity. In polyatomic molecules, it is generally thought that the lower order processes permitted by energy conservation should dominate.[29] In NM, energy conservation rules out third-order VER processes for C−H stretch decay. Fourth-order processes consistent with our observation of little or no bath excitation are

$$\nu(CH_3) \rightarrow \delta_s(CH_3) + \rho(CH_3) + \rho(NO_2)$$

$$\nu(CH_3) \rightarrow \delta_s(CH_3) + \nu_s(CN) + \delta_s(NO_2)$$

Some fifth-order processes may be equally competitive, such as

$$\nu(CH_3) \rightarrow \nu_s(CN) + \delta_s(NO_2) + 2\rho(NO_2)$$

E. Mechanisms of Subsequent VER Processes. The daughter vibrations produced by C−H stretch decay themselves decay. We broadly divide this second tier of decay processes into two parts. First, the higher energy daughter vibrations, such as the

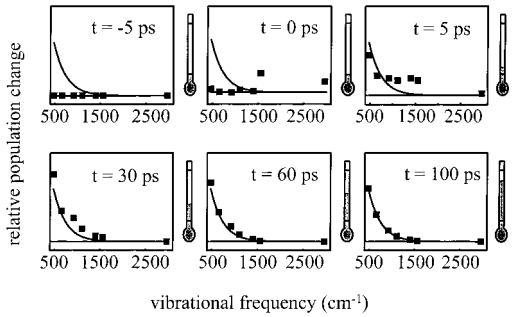

Figure 7. Time dependence of relative population changes in nitromethane after C−H stretch pumping. First overtones of the vibrations at 1560 cm^{-1} are also pumped. The symbols at 1560 cm^{-1} represent an average over antisymmetric NO_2 stretch and C−H bends. The symbols at 1400 cm^{-1} represent an average over symmetric NO_2 stretch and C−H bends. The flat line in each panel indicates the population change for the initial temperature (294 K). The curve in each panel indicates the population change expected at the final temperature. The thermometers to the right of each panel indicate the level of bath excitation.

NO_2 stretch and C−H bend in the 1560−1379 cm^{-1} range, all decay in ∼15 ps. On average, these decay processes produce about one quantum of lower energy vibrations in the 1104−480 cm^{-1} range, and the CCl_4 data in Figure 6 indicate about one-third of the total vibrational energy is dissipated to the bath. In other words, about one-third of the vibrational energy appears as phonons. Second, the lower energy daughter vibrations in the 1104−480 cm^{-1} range decay with 50−100 ps time constants, producing mainly phonons. In NM, phonon frequencies lie in the 0−160 cm^{-1} range.[19,56] The generated phonons are more likely to be in the higher frequency range because the density of states is greater and the number of phonons needed is smaller.[29]

The decay of the higher frequency vibrations must produce ∼500 cm^{-1} of phonons, which most likely means 3−4 phonons are generated. Since the parent generates one daughter plus 3−4 phonons, fifth- or sixth-order anharmonic coupling is involved. Some representative pathways would be

$$\delta(CH_3) \rightarrow \nu_s(CN) + 3-4 \text{ phonons}$$

and

$$\nu_s(NO_2) \rightarrow \delta_s(NO_2) + \rho(NO_2) + 3-4 \text{ phonons}$$

Decay of the lower energy vibrations occurs by multiphonon emission, thereby producing only phonons. In fact, it might be possible to use the techniques developed to treat multiphonon VER of diatomic molecules[9,27,57] to deal with the decay of the lowest energy vibrations in NM and other polyatomic molecules.Some examples of representative VER processes are

$$\nu_s(CN) \rightarrow 6 \text{ phonons}$$

$$\rho(NO_2) \rightarrow 3 \text{ phonons}$$

F. Overview of VC in Nitromethane. Figures 7 and 8 summarize VC in NM after C−H stretch pumping. Figure 7 is a new way of visualizing the VC process, which is made possible by combining our NM anti-Stokes data with the CCl_4 data. In Figure 7, the symbols represent population changes at the indicated value of vibrational energy relative to the change observed at the C−H stretch at t_0. The symbol at 1560 cm^{-1} represents the average of several antisymmetric C−H bending and NO_2 stretching transitions, and the symbol at 1400 cm^{-1} represents the average population change of the antisymmetric C−H bending and the symmetric C−H bending and NO_2 stretching transitions. We cannot say how the energy is partitioned among these transitions, although we believe the partitioning is relatively uniform, as mentioned earlier.

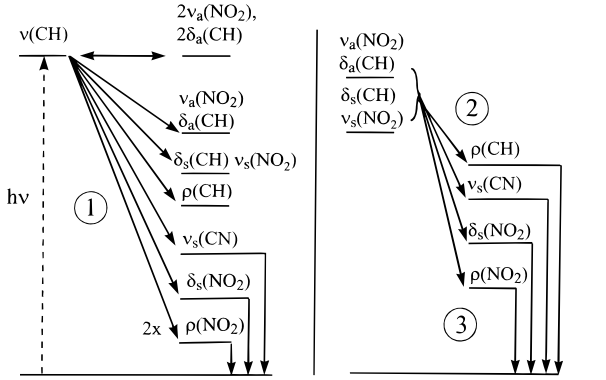

Figure 8. Energy level diagram showing the three stages of vibrational energy relaxation of nitromethane after C−H stretch excitation. The C−H stretch fundamental and the first overtones of antisymmetric C−H bends and NO_2 stretch are pumped. In stage **1**, this energy is redistributed among all other vibrations in a few picoseconds. The population increase in the lowest vibration $\rho(NO_2)$ is twice as great as the others. In stage **2**, the higher energy vibrations decay by exciting the lower energy vibrations in a few tens of picoseconds. In stage **3**, the lower energy vibrations, which build up in the first two stages, decay by exciting the bath in ∼100 ps.

In each panel of Figure 7, the line at $\Delta n = 0$ represents equilibrium at 294 K, and the curve represents the computed equilibrium distribution at the final temperature, T_f. The expected final temperature $T_f = 304$ K. The computed distribution is not sensitive to the precise value of T_f within a reasonable range. The thermometer to the right of each panel indicates the rise in bath temperature, as determined from the buildup of the CCl_4 excitation. The bottom marker on the thermometer represents the ambient temperature (294 K); the upper marker T_f.

At $t = -5$ ps, the system is in thermal equilibrium at 294 K. The pump pulse at $t = 0$ creates excess population in the C−H stretching fundamentals at ∼3000 cm^{-1} and in the overtone transitions observed at 1560 cm^{-1}. At $t = 5$ ps, the C−H stretch and the overtones at 1560 cm^{-1} have mostly decayed. Part of this decay created fundamental excitations of the ∼1560 cm^{-1} transitions, and now all other NM vibrations have become excited by fast intramolecular redistribution. The population increase in the lowest energy vibration ν_{14} is approximately twice as large as the others. Only a small fraction of the excess vibrational energy has been dissipated to the bath, as indicated by the reading of the thermometer at the right of the 5 ps panel.

At $t = 30$ ps, the higher energy vibrational populations (1400 and 1560 cm^{-1}) have decayed significantly. This decay excites lower energy vibrations, and the level of the thermometer rises to about one-third of its final value. All of the lower energy vibrational populations overshoot. "Overshoot" means the population is temporarily greater than the equilibrium population at the final temperature.[1] By $t = 60$ ps, the higher energy vibrations have almost reached equilibrium at the higher temperature. The midrange vibrations at 1100 and 918 cm^{-1} have lost most of their excess energy to the bath. The thermometer rises to about two-thirds of its final level. The overshoot of the lower energy vibrations is still in evidence.

By $t = 100$ ps, most of the system has come into equilibrium at the new, higher temperature. However, there is still a bit of excitation left in the long-lived (∼50 ps) lowest energy vibrations. That is why the thermometer to the right of this panel

has reached only about ~80% of its final reading. By $t = 150$ ps (not shown in Figure 7), the entire system has come to thermal equilibrium at 304 K.

Figure 8 is an energy level scheme for NM. It demonstrates an important result: VC in nitromethane occurs *in three distinct stages*. In the first stage, vibrational energy deposited by the laser in C−H stretches and some overtones is redistributed among essentially every vibration of NM with a 2.6 ps time constant. In the second stage, the higher energy daughter excitations populated by C−H stretch decay relax by exciting lower energy vibrations on the ~15 ps time scale. In the third stage, the long-lived lower energy vibrations, which were populated in the first two stages, relax with time constants on the order of 30−50 ps, by exciting the bath.

G. Implications for High Explosives. NM is a moderately powerful and insensitive high explosive that has been much studied because it is a homogeneous liquid,[58−61] which eliminates most of the complicated mechanical processes involved in shock initiation of solids.[62,63] We consider two roles for VER in shock initiation of NM. (1) When an initiating shock wave passes through an explosive, it excites a dense sea of phonons. These phonons must excite molecular vibrations via multiphonon up-pumping before chemical reactions can occur.[13,14,16−19,33] (2) When exothermic chemical reactions occur, highly vibrationally excited nascent products are generated. VC of these products excites phonons that drive the shock and keep it moving at a constant velocity through the explosive.[13,14] It would be interesting to see if NM is somehow different from ordinary nonexplosive polyatomic liquids.

The multiphonon up-pumping rate is inversely proportional to the population lifetimes of the lowest energy molecular vibrations,[13,14] termed "doorway modes". The general scheme first put forth by Nitzan and Jortner[64] says one should expect the doorway vibrations in polyatomic molecules to have relatively short VER lifetimes, because they should be well coupled to the strongly anharmonic bath. In our study of acetonitrile,[24] we showed this to be the case for the 378 cm^{-1} C−C≡N bending vibration, whose lifetime was less than a few picoseconds. Lifetimes of the lowest energy vibrations could not be determined for[21,22] CH_2Cl_2 or $CHCl_3$. In NM, however, the lowest energy vibrations $\delta(NO_2)$ and $\rho(NO_2)$ have long lifetimes of ~50 ps. Recent theoretical work[34] by Fried and Ruggerio suggests explosives with slower up-pumping rates (long-lived doorway modes) are more insensitive to shock initiation, and neat NM is a relatively insensitive explosive.[58,60]

In NM, the VC process takes ~150 ps, which is unremarkable, since it is similar to VC time constants observed in other polyatomic liquids such as[22] $CHCl_3$, and a bit faster than acetonitrile (~300 ps)[24] or CH_2Cl_2 (~500 ps).[21] The very rapid, nearly intramolecular VER in NM is unusual for a molecule of its size.[54] Facile intramolecular redistribution suggests that when vibrational energy enters lower frequency NM vibrations via up-pumping, the delay before the reaction coordinate becomes activated is quite short, in contrast to earlier predictions.[18] In neat NM, the first step of shock-induced reaction is thought to be breaking the C−N bond,[60] so the reaction coordinate can be associated primarily with the ~918 cm^{-1} C−N stretching vibration.

7. Conclusion and Summary

With the IR−Raman method, it is now possible to observe the entire distribution of vibrational excitation of a molecule pumped by an infrared pulse. Using the CCl_4 technique, we are now able as well to monitor the bath. Using a method for converting anti-Stokes transients to populations, we have developed a new way of visualizing the VC process (Figure 7).

In NM, VC occurs in three steps. In the first fast step, the C−H stretch (together with a small amount of overtone excitation) energy is redistributed among *all* of the other vibrations. Second, the higher frequency daughter vibrations relax by exciting lower energy vibrations. Third, the lower energy vibrations excited by the first two processes decay into the bath. The usual paradigm for VER in polyatomic molecules is the "vibrational cascade", a simple picture of vibrational energy moving down a ladder of vibrational levels,[30,31,64] which is valid when VER occurs mainly by low-order anharmonic coupling. Some of the elements of VER in NM are reminiscent of a cascade, and in earlier studies, the term was used often.[1,2,23] In NM, it is true that the highest energy excitations disappear first, followed by the middle-range excitations, followed by the lower energy vibrations. But that is not so much due to vibrational energy moving down a ladder. Instead, it is due to a fast redistribution of the vibrational energy throughout a molecule where the vibrational lifetimes *become longer* moving down the ladder. The highest energy vibrations disappear first, followed by the midfrequency vibrations, followed by the lowest frequency vibrations. Thus the idea of vibrational cascade is too simple to describe what is really happening.

Acknowledgment. This work was supported by U.S. Army Research Office contract DAAH04-96-1-0038 and Air Force Office of Scientific Research contract F49620-97-1-0056. Partial support is acknowledged from National Science Foundation DMR-9714843. L.K.I. acknowledges support from AASERT fellowships DAAHO4-95-1-0284 and DAAG55-98-1-0191.

References and Notes

(1) Chen, S.; Tolbert, W. A.; Dlott, D. D. *J. Phys. Chem.* **1994**, *98*, 7759.
(2) Chen, S.; Hong, X.; Hill, J. R.; Dlott, D. D. *J. Phys. Chem.* **1995**, *99*, 4525.
(3) Hong, X.; Chen, S.; Dlott, D. D. *J. Phys. Chem.* **1995**, *99*, 9102.
(4) Stratt, R. M.; Maroncelli, M. *J. Phys. Chem.* **1996**, *100*, 12981.
(5) Voth, G. A.; Hochstrasser, R. M. *J. Phys. Chem.* **1996**, *100*, 13034.
(6) Chesnoy, J.; Gale, G. M. *Ann. Phys. Fr.* **1984**, *9*, 893.
(7) Oxtoby, D. W. *Annu. Rev. Phys. Chem.* **1981**, *32*, 77.
(8) Oxtoby, D. W. Vibrational population relaxation in liquids. In *Photoselective Chemistry Part 2*; Jortner, J., Levine, R. D., Rice, S. A., Eds.; Wiley: New York, 1981; Vol. 47, p 487.
(9) Owrutsky, J. C.; Raftery, D.; Hochstrasser, R. M. *Annu. Rev. Phys. Chem.* **1994**, *45*, 519.
(10) Seilmeier, A.; Kaiser, W. Ultrashort intramolecular and intermolecular vibrational energy transfer of polyatomic molecules in liquids. In *Ultrashort Laser Pulses and Applications*; Kaiser, W., Ed.; Springer-Verlag: Berlin, 1988; Vol. 60, p 279.
(11) Kramers, H. A. *Physica* **1940**, *VII*, 284.
(12) Grote, R. F.; Hynes, J. T. *J. Chem. Phys.* **1981**, *74*, 4465.
(13) Dlott, D. D.; Fayer, M. D. *J. Chem. Phys.* **1990**, *92*, 3798.
(14) Tokmakoff, A.; Fayer, M. D.; Dlott, D. D. *J. Phys. Chem.* **1993**, *97*, 1901.
(15) Tarver, C. M. *J. Phys. Chem. A* **1997**, *101*, 4845.
(16) Zerilli, F. J.; Toton, E. T. *Phys. Rev. B* **1984**, *29*, 5891.
(17) Coffey, C. S.; Toton, E. T. *J. Chem. Phys.* **1982**, *76*, 949.
(18) Bardo, R. D. *Int. J. Quantum Chem.: Quantum Chem. Symp.* **1986**, *20*, 455.
(19) Bardo, R. D. The lattice density of states concept and its role in determining the shock sensitivity of PETN and nitromethane. In *Proceedings of the Ninth Symposium on Detonation*; Short, J. M., Ed., 1989; Vol. I, p 235.
(20) Eyring, H. *Science* **1978**, *199*, 740.
(21) Hofmann, M.; Graener, H. *Chem. Phys.* **1995**, *206*, 129.
(22) Graener, H.; Zürl, R.; Hofmann, M. *J. Phys. Chem.* **1997**, *101*, 1745.
(23) Deàk, J. C.; Iwaki, L. K.; Dlott, D. D. *Opt. Lett.* **1997**, *22*, 1796.
(24) Deàk, J. C.; Iwaki, L. K.; Dlott, D. D. *J. Phys. Chem. A* **1998**, *102*, 8193.

(25) Deàk, J. C.; Iwaki, L. K.; Dlott, D. D. *Chem. Phys. Lett.* **1998**, *293*, 405.
(26) Egorov, S. A.; Skinner, J. L. *J. Chem. Phys.* **1996**, *105*, 7047.
(27) Everitt, K. F.; Egorov, S. A.; Skinner, J. L. *Chem. Phys.* **1998**, *235*, 115.
(28) Califano, S.; Schettino, V.; Neto, N. *Lattice Dynamics of Molecular Crystals*; Springer-Verlag: Berlin, 1981.
(29) Kenkre, V. M.; Tokmakoff, A.; Fayer, M. D. *J. Chem. Phys.* **1994**, *101*, 10618.
(30) Hill, J. R.; Dlott, D. D. *J. Chem. Phys.* **1988**, *89*, 830.
(31) Hill, J. R.; Dlott, D. D. *J. Chem. Phys.* **1988**, *89*, 842.
(32) Velsko, S.; Oxtoby, D. W. *J. Chem. Phys.* **1980**, *72*, 2260.
(33) Pastine, D. J.; Edwards, D. J.; Jones, H. D.; Richmond, C. T.; Kim, K. Some new concepts relating to the initiation and failure of detonable explosives. In *High-pressure Science and Technology*; Timmerhaus, K. D., Barber, M. S., Eds.; Plenum: New York, 1979; Vol. 2; p 264.
(34) Fried, L.; Ruggerio, A. *J. Phys. Chem.* **1994**, *98*, 9786.
(35) Schrader, B. *Raman/Infrared Atlas of Organic Compounds*, 2nd ed.; VCH: Weinheim, 1989.
(36) Popov, E. M.; Shlyapochnikov, V. A. *Opt. Spectrosc.* **1963**, *15*, 174.
(37) Wells, A. J.; Wilson, Jr., E. B. *J. Chem. Phys.* **1941**, *10*, 314.
(38) Herzberg, G. *Molecular Spectra and Molecular Structure II. Infrared and Raman Spectra of Polyatomic Molecules*; Van Nostrand Reinhold: New York, 1945.
(39) Chen, S.; Lee, I.-Y. S.; Tolbert, W.; Wen, X.; Dlott, D. D. *J. Phys. Chem.* **1992**, *96*, 7178.
(40) Fendt, A.; Fischer, S. F.; Kaiser, W. *Chem. Phys.* **1981**, *57*, 55.
(41) Cataliotti, R.; Paliani, G. *Can. J. Spectrosc.* **1979**, *24*, 23.
(42) Cataliotti, R. S.; Foggi, P.; Giorgini, M. G.; Mariani, L.; Morresi, A.; Paliani, G. *J. Chem. Phys.* **1993**, *98*, 4372.
(43) Giorgini, M. G.; Mariani, L.; Morresi, A.; Paliani, G.; Cataliotti, R. S. *Mol. Phys.* **1992**, *75*, 1089.
(44) Giorgini, M. G.; Foggi, P.; Cataliotti, R. S.; Distefano, M. R.; Morresi, A.; Mariani, L. *J. Chem. Phys.* **1995**, *102*, 8763.
(45) Seilmeier, A.; Scherer, P. O. J.; Kaiser, W. *Chem. Phys. Lett.* **1984**, *105*, 140.
(46) Kim, H.; Dlott, D. D. *J. Chem. Phys.* **1990**, *93*, 1695.
(47) Kim, H.; Dlott, D. D. *J. Chem. Phys.* **1991**, *94*, 8203.
(48) Tokmakoff, A.; Sauter, B.; Fayer, M. D. *J. Chem. Phys.* **1994**, *100*, 9035.
(49) Hill, J. R.; Ziegler, C. J.; Suslick, K. S.; Dlott, D. D.; Rella, C. W.; Fayer, M. D. *J. Phys. Chem.* **1996**, *100*, 18023.
(50) Iwaki, L. K.; Deàk, J. C.; Rhea, S. T.; Dlott, D. D. Unpublished results, 1998.
(51) Laubereau, A.; Kaiser, W. *Rev. Mod. Phys.* **1978**, *50*, 607.
(52) Fayer, M. D. Personal communication, 1998.
(53) Quack, M. *Annu. Rev. Phys. Chem.* **1990**, *41*, 839.
(54) McDonald, J. D. *Annu. Rev. Phys. Chem.* **1979**, *30*, 29.
(55) Uzer, T. *Phys. Rept.* **1991**, *199*, 73.
(56) Cavagnat, D.; Lascombe, J.; Lassegues, J. C.; Horsewill, A. J.; Heidemann, A.; Suck, J. B. *J. Phys. (Fr.)* **1984**, *45*, 97.
(57) Harris, C. B.; Smith, D. E.; Russell, D. J. *Chem. Rev.* **1990**, *90*, 481.
(58) Campbell, A. W.; Davis, W. C.; Travis, J. R. *Phys. Fluids* **1961**, *4*, 498.
(59) Pangilinan, G. I.; Gupta, Y. M. *J. Phys. Chem.* **1994**, *98*, 4522.
(60) Gruzdkov, Y. A.; Gupta, Y. M. *J. Phys. Chem. A* **1998**, *102*, 2322.
(61) Gupta, Y. M.; Pangilinan, G. I.; Winey, J. M.; Constantinou, C. P. *Chem. Phys. Lett.* **1995**, *232*, 341.
(62) Bowden, F. P.; Yoffe, A. D. *Fast Reactions in Solids*; Academic Press Inc.: New York, 1958.
(63) Campbell, A. W.; Davis, W. C.; Ramsay, J. B.; Travis, J. R. *Phys. Fluids* **1961**, *4*, 511.
(64) Nitzan, A.; Jortner, J. *Mol. Phys.* **1973**, *25*, 713.